RSC Advances

PAPER

View Article Online
View Journal | View Issue

Cite this: *RSC Adv.*, 2017, **7**, 38367

Effect of asphaltene precipitation on CO_2-flooding performance in low-permeability sandstones: a nuclear magnetic resonance study

Chen Wang,[a] Tiantai Li,*[a] Hui Gao,[a] Jinsheng Zhao[a] and Huazhou Andy Li *[b]

With nuclear magnetic resonance (NMR), a novel experimental study is conducted to reveal the pore-scale formation damage mechanism of tight sandstones caused by asphaltene precipitation during CO_2 flooding. For each core-flooding experiment, the T_2 responses of the hydrogen nucleus in the core samples are measured before and after CO_2 flooding, and then compared to quantitatively determine the asphaltene precipitate distribution in pore throats with different sizes. It is found that in the immiscible flooding stage, the degree of asphaltene precipitation increases with an increase in the CO_2 injection pressure. After entering the miscible flooding stage, asphaltene can be still precipitated, but with a much lower magnitude. The core permeability tends to be reduced after CO_2 flooding, and the permeability reduction is positively correlated with the amount of asphaltene precipitated. The results of the NMR experiments show that during the immiscible flooding stage, oil is recovered primarily from the relatively larger pores. A small amount of asphaltene precipitation occurs in the larger pores (1–1000 ms), filling up a small portion of these pore spaces, while little asphaltene shows up in the smaller pores (0.01–1 ms). As the pressure increases beyond the minimum miscibility pressure (MMP), more oil contained in smaller pores is able to be recovered. The smaller pores tend to be more affected by the precipitated asphaltene in comparison to the larger pores. With the asphaltene-filling phenomenon taking place more in the smaller pores, the tight-core permeability can be substantially compromised after CO_2 flooding.

Received 7th June 2017
Accepted 27th July 2017

DOI: 10.1039/c7ra06392j

rsc.li/rsc-advances

1. Introduction

Tight sandstone reservoirs, a type of unconventional reservoir, are playing an important role in fulfilling the increasing energy supply over the world. Due to the unique characteristics of the tight sandstone reservoirs, including low porosity, low permeability, complex pore-throat configurations, and high heterogeneity, oil recovery from such reservoirs is rather low.[1–3]

CO_2 flooding has been widely applied to enhanced oil recovery, not only from conventional reservoirs but also from unconventional ones. Under reservoir conditions, supercritical CO_2 would interact with crude oil in the pore space, leading to significantly favorable effects such as reduced interfacial tension, reduced crude oil viscosity, and enhanced swelling of oil.[4–6] At pressures higher than the minimum miscibility pressure (MMP), a 100% oil recovery can be theoretically achieved with CO_2 flooding.[7] Hence, it is reasonable to infer that CO_2 can be a suitable agent for oil recovery in tight sandstone reservoirs. However, the performance of CO_2 flooding in tight oil reservoirs could be overshadowed by not only the fact that the injectivity of CO_2 is low in the tight sandstones, but also by the fact that the asphaltene precipitation due to CO_2–oil interaction can cause formation damage issues. Behbahani *et al.* experimentally demonstrated that during the CO_2 flooding, the injection pressure has a significant impact on the amount of asphaltene precipitated; as pressure increases, more asphaltene tends to be precipitated.[8] Such precipitated asphaltene will reduce the permeability of the core, which tends to compromise the oil recovery contributed by the enhanced CO_2 dissolution in oil.[9]

To understand the effect of asphaltene precipitation on oil recovery, extensive studies have been conducted to investigate asphaltene precipitation in high-permeability porous media due to CO_2 flooding. It has been found that when the asphaltene precipitation appears in the micro-pores in sandstone reservoirs, the larger agglomerates will block up the pore throat directly, while the smaller ones will cause a blockage of the pore throat through a bridging effect at the throat.[10] Both of these effects can lead to a significant decrease in permeability, and thus decrease the overall oil recovery during CO_2 flooding.[11–13] Papadimitriou *et al.* reported that the precipitated asphaltene will clog the reservoir pores and lead to a 40–90% decrease in permeability.[14] Much less research has been conducted to

[a]*School of Petroleum Engineering, Xi'an Shiyou University, Xi'an, China 710065. E-mail: ttli@xsyu.edu.cn*

[b]*School of Mining and Petroleum Engineering, Faculty of Engineering, University of Alberta, Edmonton, Canada T6G 1H9. E-mail: huazhou@ualberta.ca; Fax: +1-780-492-0249; Tel: +1-780-492-1738*

understand the effect of asphaltene precipitation on CO_2 flooding performance in low-permeability sandstones compared the extensive researches that have been dedicated to the high-permeability sandstones. Wang *et al.* demonstrated that, during immiscible CO_2 flooding, an increase in the injection pressure results in an increase in the oil recovery factor, which is nevertheless accompanied by an decreased permeability due to the increased amount of asphaltene precipitated at higher pressures; the amount of asphaltene precipitated keeps increasing even after the injection pressure is higher than the MMP, albeit with a lessened degree.[15] Cao and Gu showed in their experiments that the oil recovery increases monotonically as the injection pressure increases in the immiscible flooding because of the increased CO_2 dissolution in the crude oil. When the injection pressure exceeds the MMP, the oil recovery increases slightly and reaches the maximum afterwards at a higher pressure. In addition, it is observed that the amount of asphaltene precipitation increases continuously in the immiscible and miscible region, and similar observations can be made with regard to the variation trend of the core permeability.[16] What is lacking in the previous research is that no investigation has been made to quantify how the asphaltene blocks the pores with different sizes.

It is worthwhile mentioning that, in addition to the asphaltene precipitation issue, another process, *i.e.*, the CO_2/rock reactions may also reduce the sandstone permeability. Yu *et al.* conducted an experimental study of CO_2/brine/sandstone interaction under *in situ* pressure/temperature reservoir conditions. It was found that carbonate materials in the natural core, such as calcite and ankerite, were dissolved during the CO_2/rock reactions; as a result, solid precipitates and clays (*e.g.*, kaolinite) were generated. The solid precipitates and clay particles will migrate into the pore space and possibly accumulated at pore throats, leading to a significant decrease in permeability.[17] Mohamed *et al.* experimentally demonstrated that, the CO_2/rock reactions bring about 35% to 55% loss in core permeability during the CO_2 injection in the sandstone reservoirs.[18] Other studies have reported similar findings. But it is noted that all these studies have used natural cores that are retrieved from hydrocarbon reservoirs. Since the natural cores contain feldspars, calcite and ankerite, the asphaltene precipitation and CO_2/rock reactions will both take place during CO_2 flooding of the natural cores. Therefore, the use of natural cores to investigate the effect of asphaltene precipitation makes it hard to delineate the individual contributions of asphaltene precipitation and CO_2/rock reactions towards the permeability reduction. In this research, we are able to elucidate the sole impact of asphaltene precipitation on permeability reduction. We have excluded the effect of CO_2/rock reactions by using artificial core samples which do not contain carbonate cementing materials. In addition, there is no quantitative investigation in previous research with regard to: (1) how the asphaltene precipitation alters the pore structures with different sizes; (2) how pore-structure variation results in decreased permeability; and (3) how such pore-structure variation influences the recovery of oil residing in different pores by CO_2 injected. Therefore, it is of great importance to understand the sole influence of asphaltene precipitation on the alteration of pore size distribution and thereby the permeability reduction of core samples during CO_2 flooding.

In this study, tight artificial cores are used in the experiment to make sure that the change of permeability is only caused by asphaltene precipitation. The cores used consist only of quartz, which ensures that no CO_2/rock reactions will occur during a CO_2 flood. Eight CO_2 core-flooding tests are conducted at the immiscible, near-miscible and miscible conditions. During these tests we measure the oil recovery factors, the amount of asphaltene precipitated, and the decrease in permeability. To elaborate on the detailed mechanisms of the reduction in permeability due to asphaltene precipitation, the nuclear magnetic resonance (NMR) is employed to quantitatively evaluate the distribution of asphaltene precipitation in the pore-throat configurations. ^{1}H NMR relaxometry has found extensive applications in exploring surface interactions in catalysts[19] as well as characterizing the properties of porous materials such as metal–organic frameworks,[20] silica gels, zeolites, cement, cellulose fibers and rock samples.[21] To our knowledge, this study is the first attempt to quantitatively evaluate the effect of CO_2 flooding on asphaltene precipitation on the microscopic pore-structure alterations with the aid of NMR technique.

2. Experimental section

2.1 Materials

The cores used in this experiment are the low-permeability artificial cores (cementation of quartz) manufactured from Northeast Petroleum University in China. The artificial cores are prepared with cement and quartz. The following cement/quartz ratios are used: cement weight percentage between 5–15 wt% and quartz weight percentage between 85–95 wt%. Epoxy resin and three additives (dibutyl phthalate, ethylenediamine and acetone) are added into the cement according to following recipe: 0.5 to 1.5 wt% of epoxy resin, 0.1 to 0.5 wt% of dibutyl phthalate, 0.01 to 0.1 wt% of ethylenediamine, and 0.1 to 1.0 wt% of acetone. The process for the core preparation is described as follows: (1) first, stir the quartz sand and cements evenly, and then place the mixture into a mold; (2) place the mold on a press and apply a pressure of 8.3 MPa to press the mold for 15 min; (3) next, place the compressed core in an oven and heat it at 85 °C for 8 h; (4) after heating, move the core out of the oven and let it cool down under room conditions; (5) after being left alone for 48 hours, the core can be used to conduct the flooding experiments. The properties of the cores are listed in Table 2.

The crude oil is collected from Jiyuan oilfield in Ordos basin, China. The density and viscosity of the crude oil sample are measured to be 760 kg m^{-3} and 1.6 mPa s at reservoir conditions of 80 °C and 15 MPa. The asphaltene content of the crude oil is measured to be 1.15 wt% (*n*-pentane insoluble). Before performing the experiments, wax and SARA (saturates, aromatics, resins and asphaltenes) contents in the oil sample are also measured. The wax content is measured by the thin-layer chromatography/flame ionization detection (TLC-FID) method, while the SARA analysis is conducted using the thin-

Table 1 Asphaltenes, resins and waxes contents of the crude oil sample

Component	Asphaltenes	Resins	Waxes
Weight percentage	1.15 wt%	0.14 wt%	0.11 wt%

layer chromatography (TLC).[22,23] Wax, asphaltenes and resins are the typical materials found in crude oil that can be precipitated at specific conditions. Table 1 shows the measured contents of wax, asphaltenes and resins. The effect of wax/resins precipitation can be neglected due to their relatively low concentrations in the oil sample. Furthermore, the experimental temperature in this study is maintained at 80 °C which is much higher than the wax appearance temperature. Therefore, the chance of wax precipitation occurring in the core sample is extremely low.

The manually prepared water has a salinity of 30 000 mg L^{-1}, a salt type of $CaCl_2$, and viscosity of 0.4 mPa s at 80 °C and 15 MPa. It is used in the experiments to simulate the formation water. CO_2 with a purity of 99.9% is supplied by Xi'an Specific Standard Coal Gas Supply Station (China).

2.2 Experimental setup

The experimental setup used for conducting the core flood experiments is provided in Fig. 1. A syringe pump (ISCO-260D, Teledyne Isco, Lincoln, NE, America) is used to inject the crude oil, formation water or CO_2 from the high pressure cylinders (Huaxing Co., Nantong, China) to the core holder (Huaxing Co., Nantong, China) which is a special core holder used for NMR setup. The ISCO-260D syringe pump has a pressure range of 0–51.7 MPa and a rate range of 0.001–80 mL min^{-1}. The core holder can be operated at a pressure of 50 MPa and a temperature of 150 °C. The back pressure is controlled by a back-pressure regulator (BPR-50, Temco, USA) and the gas production volume is measured by a gas flow meter (Puttom Co., Beijing, China). An electric heater (Huaxing Co., Nantong, China) is used to heat the oven and maintain the temperature at 80 °C.

The NMR apparatus (Mini-MR, Niumag, China) is purchased from Suzhou Niumag Corporation, China (http://en.niumag.com). Its magnetic intensity, gradient value and frequency range are 0.5 T, 0.025 T m^{-1} and 1–30 MHz, respectively. Its control precision is 0.01 MHz. The parameters of the NMR apparatus are set as follows: T_e (time of echo), 0.27 ms; T_w (time of wait), 4000 ms; N_{ech} (number of echo), 6000; N_s (number of scan), 64; the pulse width is divided into 90° pulse width ($P_1 = 22$) and 180° pulse width ($P_2 = 40$). For precision control purpose, calibration of the NMR apparatus is required prior to each measurement. The calibration is deemed to be acceptable if the NMR is able to detect the T_2 signal of a 10 mg water film.

2.3 Experimental procedures

2.3.1 Measurement of asphaltene content. We use the UV-VIS-NIR spectrophotometer to measure the asphaltene content (UV-3600 Plus, Shimadzu Corporation, Japan). This test method requires a small amount of oil. The amount of oil produced during the experiments is small, making the spectrophotometer an ideal tool for conducting such measurement. The measurement is conducted under room temperature and pressure. The procedure for determining the asphaltene content using the spectrophotometer is as follows: (1) dissolve 0.1000–1.000 g of crude oil sample into 1.00 mL of toluene; (2) prepare 100.00 mL of *n*-heptane and heat it to 85 °C; (3) pour the *n*-heptane into the oil/toluene mixture and vigorously stir the resulting mixture until a homogenous suspension is obtained; (4) cool the suspension to room temperature; (5) meanwhile, prepare 100.00 mL of *n*-heptane as a reference fluid; and (6) under wavelengths of 750 nm and 800 nm, use the UV-VIS-NIR spectrophotometer to measure the absorbance of the suspension contained in a 1 cm quartz bath, which eventually determines the asphaltene content in the crude oil sample.

2.3.2 MMP test. We first measure the MMP of the crude oil sample. At present, there are two major methods to determine the MMP for a given crude oil–CO_2 system, *i.e.*, the rising-bubble apparatus (RBA) test and the slim-tube test.[24,25] Recently, Hawthorne *et al.* developed another convenient method, so-called capillary rise/vanishing interfacial tension method, for measuring MMP.[26] In this study, the slim-tube test, which is the most reliable and commonly used among the experimental methods, is applied to determine the MMP.

The slim tube test apparatus is composed of three parts: the injection system, the slim tube and the production system. The slim tube, which is filled with quartz sand, has a length of 20 m

Table 2 Physical properties of the core samples and summary of the CO_2 flooding experiments conducted at 80 °C

Core sample	1	2	3	4	5	6	7	8
Length (mm)	200.2	200.0	200.1	200.5	199.2	199.9	200.3	200.0
Core radius (mm)	25.1	25.0	24.9	24.7	25.0	25.0	25.1	25.4
Porosity (%)	4.8	4.5	4.6	4.5	4.4	4.5	4.8	4.7
Injection pressure (MPa)	4.6	7.2	8.5	15.2	20.7	23.2	25.5	35.2
Permeability (mD)	0.22	0.21	0.22	0.22	0.22	0.21	0.22	0.22
Relative reduction in the permeability (%)	0	9.09	13.63	18.18	27.27	36.36	40.91	45.45
Percentage of asphaltene precipitated after 7 PVs of CO_2 injection (%)	12.56	15.18	17.33	22.23	24.23	30.91	33.15	36.26
Final oil recovery after 7 PVs of CO_2 injection (%)	27.35	44.05	56.11	61.17	81.65	85.90	87.98	89.12

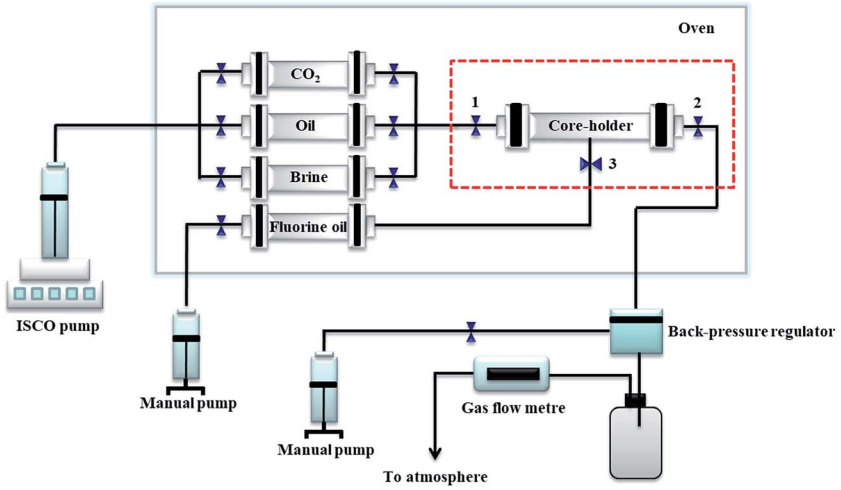

Fig. 1 Schematic of the coreflooding apparatus used for the coreflooding experiments.

and a diameter of 3.75 mm. Before the measurements, the tube is cleaned and dried at 100 °C for 6 h in the oven. Then we measure the air permeability and porosity of the slim tube. The experimental temperature is set to 80 °C and the pressure levels considered in this research include the following: 14 MPa, 18 MPa, 22 MPa, 26 MPa, and 30 MPa. The oil displacement efficiency is found to be less than 90% at two pressure points (14 MPa and 18 MPa) but higher than 90% at the other three pressures.[27,28] During the test, the injection rate is maintained at 0.125 mL min^{-1}. But when the gas breaks through, this rate cannot maintain a constant injection pressure; so we properly increase the injection rate to maintain a constant injection pressure in this case. We terminate the slim tube experiment when the volume of CO_2 reaches 1.2 times of the core's pore volume (PV). Finally, the pressure-recovery curve is drawn and analyzed to determine the MMP.

2.3.3 Coreflooding experiments. The experimental procedure is described as follows:

(1) The artificial core samples are cleaned and dried at 100 °C for 8 h in the oven. The air permeability is measured by a gas permeameter (Ultraperm – 500 TM, TEMCO, USA).

(2) In order to saturate the core, the core is placed in a sealed container and emerged in the simulated formation water. The sealed container is vacuumed for 24 h under a pressure of −80 kPa, allowing formation water to enter the core sample. Once the core weight remains unchanged the water saturation process is deemed to be terminated. To calculate the porosity, the core is weighed before and after water saturation. The following equation is used to calculate the porosity on the basis of the weight difference of the core before and after water saturation,

$$V_C = V_W = \frac{M_2 - M_1}{\rho_w} \quad (1)$$

where V_c is the pore volume of core sample; V_w is the volume of water vacuumed into the core sample; M_1 is the weight of the core sample before water saturation; and M_2 is the weight of the core after water saturation. Then the porosity can be calculated by,

$$\phi = \frac{V_C}{V} \quad (2)$$

where V is the volume of core sample and ϕ is the porosity of the core sample.

(3) At this point, the core sample is also scanned by the NMR apparatus to obtain a T_2 response under initial water-saturated condition.

(4) The core is displaced with the $MnCl_2$ solution (15 000 mg L^{-1}) by 3–4 PV in order to eliminate the hydrogen signal of brine. After the displacement the core sample is scanned again by the NMR apparatus.

(5) The core sample is placed in a core holder, and the oil is injected into the core sample with an injection rate of 0.01 mL min^{-1} until water cut is less than 1%. Upon the end of oil saturation, the T_2 response of the core sample is measured again.

(6) CO_2 is injected into the core sample at a constant rate of 0.5 mL min^{-1} at 80.0 °C to conduct experiments at eight pressures of 4.6 MPa, 7.2 MPa, 8.5 MPa, 15.2 MPa, 20.7 MPa, 23.2 MPa, 25.5 MPa, and 35.2 MPa. These pressures are maintained by the back-pressure at the rear of the core holder. The back-pressure is kept 1.0 MPa lower than the injection pressure.

(7) The injection pressure, injection rate, confining pressure and back pressure are all recorded. We collect the produced oil and gas. When the amount of CO_2 injected reaches 7 PV, the displacement is completed and the asphaltene content of the produced oil is measured by a spectrophotometer.

(8) After the CO_2 flooding test, the core samples are cleaned with benzene and dried at 100 °C for 12 h in the oven. Afterwards, its permeability and porosity are measured again.

(9) After CO_2 flooding test, the core sample undergoes the same treatments as described from step 1 to step 4. Eventually, another NMR scan is used to reveal the oil distribution across the different pores of the core sample. It is noted that the NMR scan is also made again in the step 2.

As shown in Fig. 1, to conduct a NMR scan we close valves #1, #2 and #3, decouple the core holder from the flooding

apparatus and then place it in the NMR apparatus for T_2 scan. The coreflooding apparatus and the NMR apparatus are placed in the same room 2 m apart and thus the nonmagnetic core holder can quickly loaded to the NMR apparatus for testing. The time needed for handling the core holder and conducting NMR scans is relatively short (maximum several minutes), and therefore fluid shrinkage in the core can be ignored.[29] These measures greatly minimise the chance of isolation/depressurization and cooling occurring in the core holder during the NMR scan.

2.3.4 NMR tests. The NMR apparatus used in this study detects the transverse relaxation motion of the ^{1}H of fluids in the pores. The oil distribution in the pore throats can be obtained by detecting the ^{1}H in the oil molecules. The magnitude of the T_2 response represents the relative amount of oil present in the porous media.

The total T_2 response of fluids in the tight core samples is given as,[30,31]

$$\frac{1}{T_2} = \frac{1}{T_{2S}} + \frac{1}{T_{2D}} + \frac{1}{T_{2B}} \quad (3)$$

where T_{2S} is the transverse relaxation time from the core surface; T_{2D} is the transverse relaxation time due to the fluids diffusion in magnetic gradients; and T_{2B} is transverse relaxation time from the bulk relaxation.

For fluids flow in the core samples, the transverse relaxation time due to the fluids diffusion (T_{2B}) and due to the bulk relaxation (T_{2D}) can be reasonably neglected, that is, only the relaxation time from the core surface (T_{2S}) mainly contributes to the total T_2 response.[29] Furthermore, the rock-surface relaxation strongly correlates with the specific area of the rock sample, which is defined as the ratio of the surface area of a pore to the volume of the same pore. A larger specific area can result in a stronger T_2 relaxation but a smaller T_2 relaxation time. Therefore, the T_2 response can be expressed as,[32,33]

$$\frac{1}{T_2} \approx \frac{1}{T_{2S}} = \rho\left(\frac{S}{V}\right) \quad (4)$$

where ρ presents the surface relaxation rate (μm ms^{-1}); and (S/V) represents the specific area of the core sample (1/μm), *i.e.*, the ratio of the total surface area from the pores to the total pore volume of the core sample. The specific area of the core sample correlates with the pore throat radius and therefore eqn (4) can be directly converted to,[30,31]

$$T_2 = \frac{1}{\rho F_s} r \quad (5)$$

then,

$$r = CT_2 \quad (6)$$

where F_S is the dimensionless shape factor of the pores present in the core sample and r is the pore throat radius (μm). It can be seen from eqn (6) that if $C = 1/(\rho F_S)$ is considered to be a constant,[29,34,35] the T_2 response is directly proportional to the pore throat radius. The higher the T_2 value is, the larger the pore throat radius will be. The T_2 response of all core samples is mainly distributed in the range of 0.01–1 ms and 1–1000 ms. In our work, we define the 0.01–1 ms as the smaller pores and the 1–1000 ms as larger pores.

3. Results and discussion

3.1 CO_2–oil MMP

The recovery factor of the slim tube test is described in Fig. 2. At injection pressures lower than the MMP (14.0 MPa and 18.0 MPa), it can be found that the recovery factor increases rapidly from 60.23% to 79.18% as the injection pressure increases. This corresponds to a typical immiscible flooding stage. When the injection pressure is higher than 21.6 MPa, the oil recovery factor is more than 90% and increases slowly as the pressure increases, indicating a miscible flooding stage. As such, the MMP of the crude oil can be determined to be 21.6 MPa since this pressure corresponds to the breakpoint of the oil recovery curve and the recovery factor at this pressure is above 90%.[36,37]

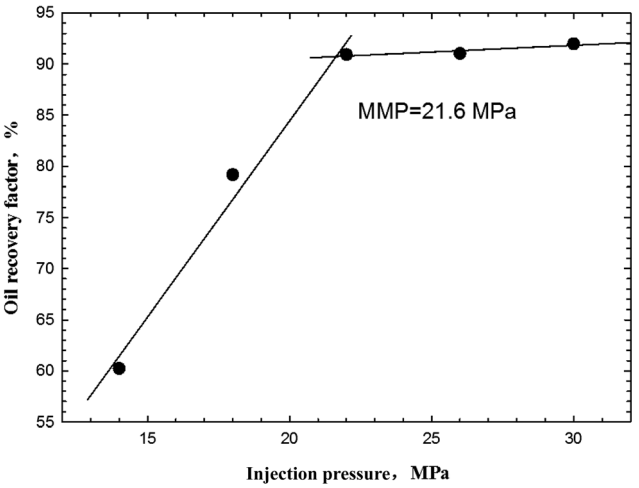

Fig. 2 Determination of the MMP of the crude oil–CO_2 system on the basis of the slim tube test.

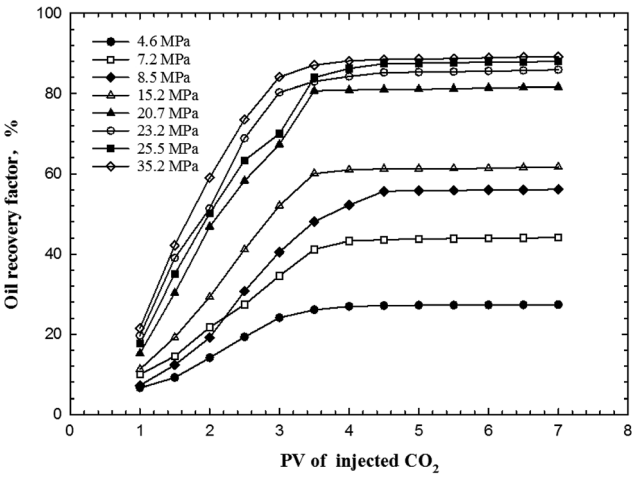

Fig. 3 Oil recovery factors as a function of the injected PVs of CO_2 at different pressures.

We also compare this measured MMP to the MMP calculated by an empirical correlation. The CO_2–oil MMP correlation was initially proposed by Alston *et al.* and improved by Li *et al.*[37,38] Using this correlation, the MMP is calculated to be 20.5 MPa, showing a 5% relative deviation from the measured MMP.

3.2 Oil recovery due to CO_2 flooding

3.2.1 Oil recovery profiles. Table 2 shows the physical properties of the core samples used in the CO_2 flooding experiments and summaries the major results of the CO_2 flooding experiments. It is noted that the injection pressure ranges from 4.6 MPa to 35.2 MPa, which covers all the immiscible, near-miscible, and miscible conditions. Fig. 3 shows the oil recovery factors as a function of the PVs of CO_2 injected at different pressures.

It can be seen from Fig. 3 that when the volume of CO_2 injected changes from 1 PV to 4 PV, the oil recovery increases rapidly. Afterward, the oil recovery only increases slightly with a further increase in the CO_2 injection volume. Fig. 4 shows the oil recovery factors achieved after 7.0 PVs of CO_2 injection *vs.* the CO_2 injection pressure. As seen from Fig. 4, the oil recovery factor tends to increase quickly with an increase in pressure in the immiscible flooding stage. In the immiscible flooding stage, CO_2 density increases sharply as pressure increases, leading to faster dissolution of CO_2 in crude oil contained in the core sample. The large amount of CO_2 dissolved in the crude oil reduces the viscosity of the crude oil, reduces the interfacial tension between CO_2 and oil, and swells the volume of the crude oil.[6,15] All these beneficial effects lead to a quick recovery of oil in this stage. After entering the miscible flooding stage, these beneficial effects are diminishing, leading to only a slight increase in the recovery factor. Overall, the recovery curve, which is obtained by the CO_2 coreflooding experiments, echoes well with that obtained by the slim tube experiments.

3.2.2 Comparison of T_2 response measured for the initial oil-saturated core and that measured for the core immediately after CO_2 flooding. Three cores, which have undergone CO_2 flooding at the injection pressures of 4.6 MPa (immiscible state), 20.7 MPa (near-miscible state) and 35.2 MPa (miscible state), respectively, are selected for conducting the NMR tests.

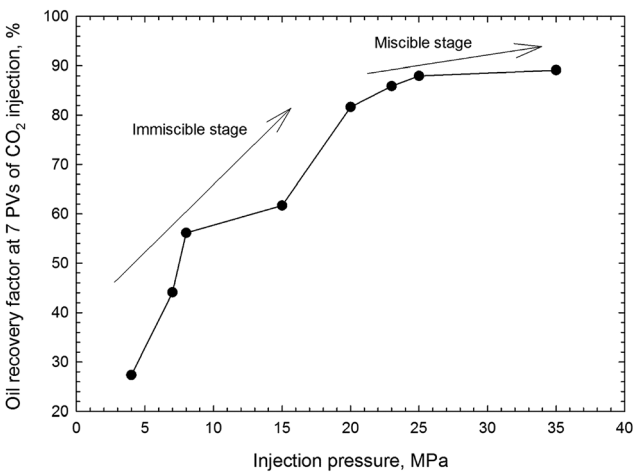

Fig. 4 Oil recovery factors achieved after 7.0 PVs of CO_2 injection *vs.* the CO_2 injection pressure.

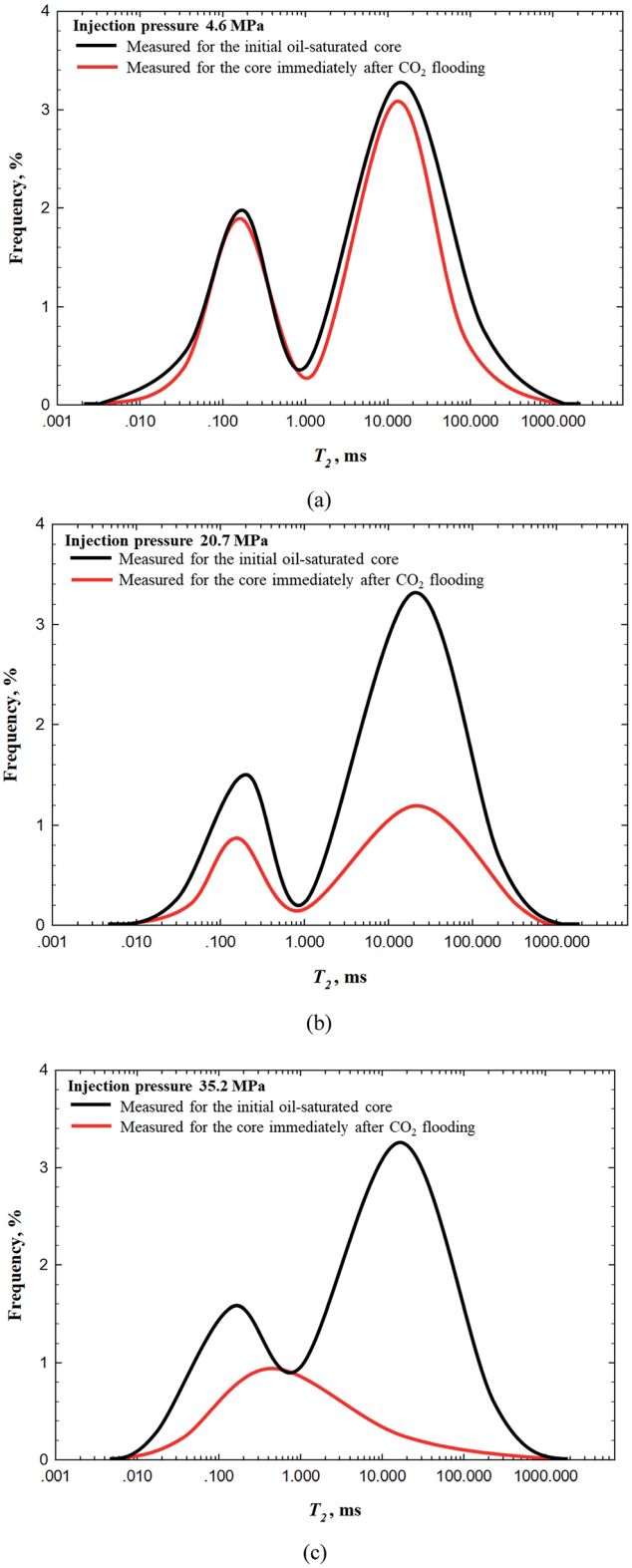

Fig. 5 Measured T_2 responses of core samples before and after the CO_2 flooding conducted at: (a) 4.6 MPa; (b) 20.7; and (c) 35.2 MPa.

Fig. 5 illustrates the T_2 responses of the three cores before and after CO_2 flooding conducted at 4.6 MPa, 20.7 MPa and 35.2 MPa, respectively. In order to compare the variation of T_2 responses scanned at different times, the following normalization equation is used when plotting Fig. 5,

$$f = \frac{A}{S} \tag{7}$$

where f is T_2 frequency; A is the original values of T_2 amplitude measured by each NMR scan; and S is the summation of T_2 amplitudes measured for the initial oil-saturated core.[29] It can be observed from Fig. 5 that the T_2 response under the initial saturated oil condition is mainly bimodal. It should be noted that the area covered by the T_2 response stands for the relative oil contents in the core, and a larger coverage area indicates higher oil content.

T_2 profiles with different levels of intensity are detected at the end of the various CO_2 flooding experiments. As for these three cases, the drops in the right peak of the T_2 response are all more obvious than that in the left peaks of the T_2 response. This indicates that the oil in the larger pores (1–1000 ms) can be more easily accessed and recovered by the injected CO_2 than that in the smaller pores (0.01–1 ms). The left peak of the T_2 response for the core #1 exhibits a smaller drop. It means that less oil in small pores (0.01–1 ms) has been displaced and recovered by CO_2. Based on these observations, we can infer that, compared to the larger pores (1–1000 ms), the smaller pores (0.01–1 ms) can be more easily blocked/filled by the asphaltenes that are precipitated during the CO_2 flooding process.

3.3 Asphaltene precipitation and permeability reduction

The percentage of asphaltene precipitated is calculated by comparing the asphaltene contents in the original oil sample and the produced oil, while the percentage of permeability reduction is calculated by comparing the permeability of the core before and after CO_2 flooding, while. The following equation is used to calculate the percentage of asphaltene precipitation,

$$A = \frac{C_1 - C_2}{C_1} \times 100\% \tag{8}$$

where A is the percentage of asphaltene precipitation, %; C_1 is the asphaltene content of the initial oil, %; and C_2 is the asphaltene content of the produced oil, %. The following equation is used to calculate the percentage of permeability reduction,

$$P = \frac{K_1 - K_2}{K_1} \times 100\% \tag{9}$$

where P is the percentage of permeability reduction, %; K_1 is the initial permeability of the core sample, mD; and K_2 is the permeability of the core sample after each flooding, mD.

Table 2 also shows the percentage of asphaltene precipitated as well as the relative reduction in the permeability after each flooding experiment. At an injection pressure of 4.6 MPa, asphaltene precipitation first appears, leading to that the asphaltene content in the produced crude oil is reduced compared to that in the original oil sample. Fig. 6 plots the percentage of asphaltene precipitated after 7 PVs of CO_2 injection and the relative permeability reduction of the core samples at different injection pressures. It can be seen from Fig. 6 that, in the immiscible flooding stage, the amount of asphaltene precipitation tends to significantly increase as the pressure increases. When the injection pressure rises above the MMP, we can still observe asphaltene precipitation after the CO_2 flooding experiments, but such precipitation is much less compared to that resulted from the immiscible flooding. These findings are generally consistent with those reported in Wang and Gu.[15]

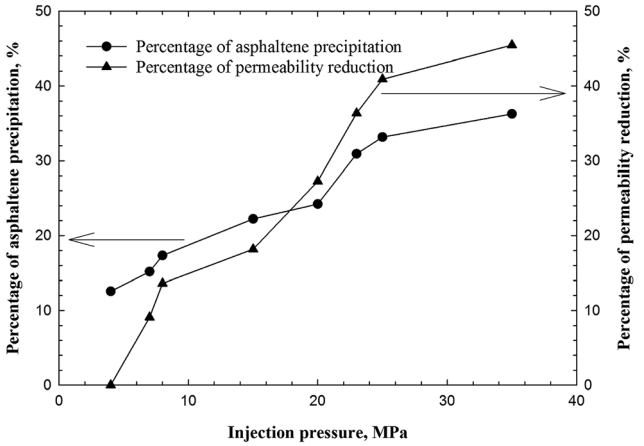

Fig. 6 The percentage of asphaltene precipitated and the relative reduction in permeability of the core samples at different injection pressures.

Similarly, the permeability of the core samples is seen to decreases with increased injection pressure. This is attributed to the fact that the amount of asphaltene precipitated in the core samples is increased as pressure increases. It can be observed from Fig. 6 that the degree of permeability reduction is positively correlated with the percentage of asphaltene precipitated. In the immiscible flooding stage, an increase in pressure results in more severe asphaltene precipitation. With more asphaltene precipitated, more pore spaces can be blocked by the asphaltene. As a result, a more severe reduction in the core permeability ensues. A question arises here with regard to how the asphaltene precipitation has blocked the pore spaces in the core sample, and thereby altered the pore size distribution of the core sample. This will be addressed by the NMR tests discussed in Section 3.4.

3.4 Effect of asphaltene precipitation on NMR responses

3.4.1 Comparison of T_2 response measured for the initial water-saturated core and that measured for the water-saturated core after CO_2 flooding. As mentioned in the experimental procedure, we also measure the T_2 response for the initial water-saturated core and the T_2 response for the water-saturated core after CO_2 flooding. Fig. 7 plots the T_2 response measured under different experimental scenarios. It can be seen from Fig. 7 that the bimodal distributions as show in Fig. 5 have been altered to

be unimodel distributions. The reason, leading to that we are only able to detect the NMR response from large pores, is that the core sample is being saturated with water through vacuuming forces. It can be observed from Fig. 7 that, being vacuumed into the core sample, water is only filling up the

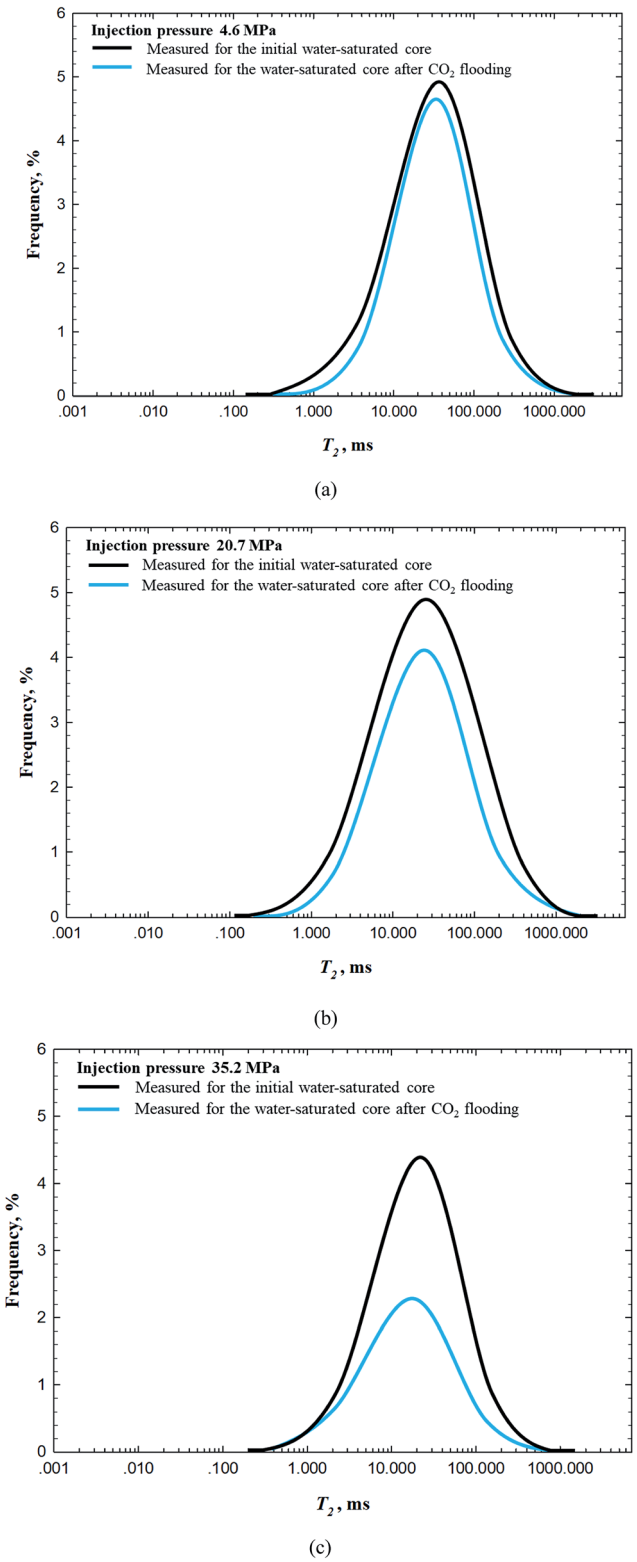

Fig. 7 Comparison of the T_2 response measured for the initial water-saturated core and for the water-saturated core after CO_2 flooding conducted at: (a) 4.6 MPa; (b) 20.7 MPa; and (c) 35.2 MPa.

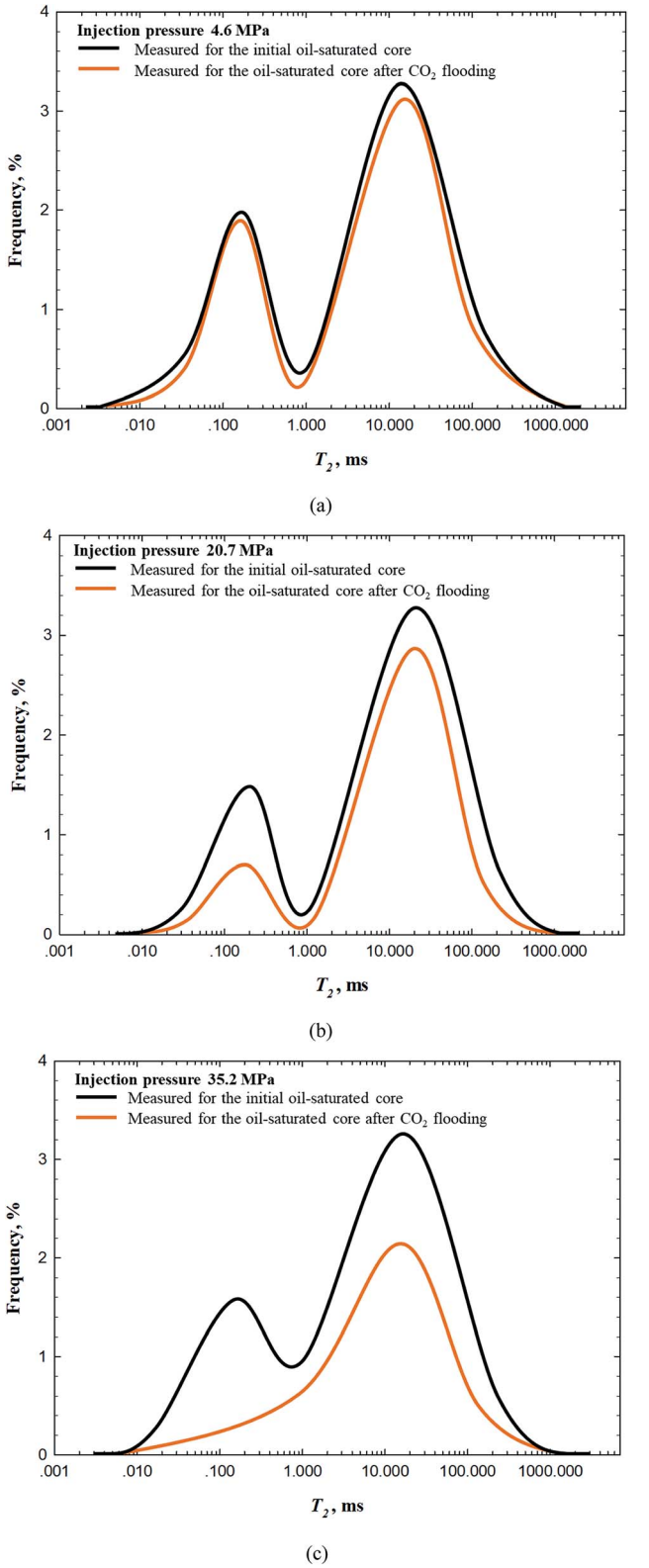

Fig. 8 Comparison of T_2 response measured for the initial oil-saturated core and that measured for the oil-saturated core after CO_2 flooding conducted at: (a) 4.6 MPa; (b) 20.7 MPa; and (c) 35.2 MPa.

larger pores corresponding to T_2 response between 1–1000 ms. The vacuuming force cannot imbibe water into the smaller pores corresponding to T_2 response between 0.01–1 ms.

It can be observed from Fig. 7(a) that the T_2 response measured for the water-saturated core after CO_2 flooding (4.6 MPa) moves to a slightly lower position compared to that measured for the initial water-saturated core. This indicates, after CO_2 flooding, a small portion of the larger pores is clogged by the asphaltene precipitated. The blockage of the larger pores becomes more severe when the CO_2 flooding is conducted at higher pressures, as illustrated by Fig. 7(b) and (c).

3.4.2 Comparison of T_2 response measured for the initial oil-saturated core and that measured for the oil-saturated core after CO_2 flooding. When we are saturating the core with the oil sample, the oil is injected into the core by the syringe pump. The injection force exerted by the pump has enabled the crude oil to enter both the larger pores and smaller pores, leading to the appearance of the bimodal T_2 response as shown in Fig. 5. To reveal the effect of asphaltene precipitation on the blockage of both smaller pores (0.01–1 ms) and larger pores (1–1000 ms), we measured the T_2 responses for the initial oil-saturated core and for the oil-saturated core after CO_2 flooding. The difference between the two T_2 responses can reflect how much of the pore system have been filled with the asphaltene precipitated. The results are plotted in Fig. 8. As shown in Fig. 8(a), the amount of saturated crude oil in the core sample has decreased in both larger and smaller pores, indicating that asphaltene tends to block the pore spaces after CO_2 flooding conducted at 4.6 MPa; but at such low injection pressure, a small portion (about 4.50%) of the large pores (1–1000 ms) is filled up with the asphaltene precipitated, while only a tiny part of the smaller pores (0.01–1 ms) is filled up with the asphaltene precipitated. However, when the injection pressure increases above the MMP, an opposite trend can be observed from Fig. 8(b): more than 43.21% of the smaller pores (0.01–1 ms) is clogged, while only 15.62% of the large pores (1–1000 ms) is affected by the asphaltene. It can be seen from Fig. 8(c) that as the pressure further increases to 35.2 MPa, 72.32% of the smaller pores (0.01–1 ms) and 38.69% of large pores (1–1000 ms) are, respectively, blocked by the asphaltene precipitated during CO_2 flooding. In addition, after CO_2 flooding conducted at such a high injection pressure, the left peak in the T_2 response completely disappears, implying that the large amount of asphaltene precipitated during the miscible CO_2 flooding has blocked the majority of the smaller pores. Such consequences can lead to a substantial decrease in the core permeability, as mentioned above.

4. Conclusions

We conduct an experimental study to reveal the formation damage mechanism of tight cores due to asphaltene precipitation during CO_2 flooding. Because of the use of artificial tight cores, we make sure that only asphaltene will be the major solid phase that is precipitated during CO_2 flooding, while the solid precipitation due to CO_2/rock reactions is excluded. The following conclusions can be obtained from the study:

•In the immiscible flooding stage, the degree of asphaltene precipitation increases with an increase in the CO_2 injection pressure. After entering the miscible flooding stage, asphaltene can be still precipitated, but with a much lower magnitude. The reduction in the core permeability after CO_2 flooding shows a similar dependence on CO_2 injection pressure.

•A comparison is made between the T_2 response measured for the initial oil-saturated core and the T_2 response measured for the core immediately after CO_2 flooding. It is found that, in the immiscible flooding stage, the oil recovery mainly originates from the recovery of the oil that is contained in the relatively larger pores. As the pressure increases beyond the MMP, more oil contained in the smaller pores is able to be tapped.

•We also compare the T_2 response measured for the initial water-saturated core and the T_2 response measured for the water-saturated core after CO_2 flooding. The comparison shows that in the immiscible flooding stage, a small amount of asphaltene precipitation occurs in the larger pores (1–1000 ms), filling up small portion of these pore spaces, while little asphaltene shows up in the smaller pores (0.01–1 ms). In the miscible flooding stage, the smaller pores tend to be more affected by the precipitated asphaltenes compared to the larger pores, leading to a substantial decrease in the core permeability.

Acknowledgements

C. Wang thanks the visiting PhD scholarship provided by the China Scholarship Council (CSC) for supporting his stay at the University of Alberta. The authors also acknowledge the editorial assistance provided by Sean Perkins in preparing the manuscript.

References

1 D. J. Soeder and P. L. Randolph, *SPE Form. Eval.*, 1987, **2**, 129–136.
2 P. H. Nelson, *AAPG Bull.*, 2009, **93**, 329–340.
3 L. Xiao, C. C. Zou and X. H. Xie, *Australian Society of Exploration Geophysicists*, 2016, 575–580.
4 K. Asghari, M. Dong, J. Shire, T. Coleridge, J. Nagrampa and J. Grassick, *SPE Prod. Oper.*, 2007, **22**, 260–264.
5 Y. C. Zhao, Y. C. Song, Y. Liu, H. F. Liang and B. L. Dou, *Ind. Eng. Chem. Res.*, 2011, **50**, 4707–4715.
6 H. Z. Li, S. Zheng and D. Yang, *SPE J.*, 2013, **18**, 695–707.
7 H. Z. Li, J. S. Qin and D. Y. Yang, *Ind. Eng. Chem. Res.*, 2012, **51**, 3516–3523.
8 T. J. Behbahani, C. Ghotbi, V. Taghikhani and A. Shahrabadi, *Energy Fuels*, 2012, **26**, 5080–5091.
9 R. K. Srivastava, S. S. Huang and M. Dong, *SPE Prod. Facil.*, 1999, **14**, 235–245.
10 Y. F. Hu, S. Li, N. Liu, Y. P. Chu, S. J. Park, G. A. Mansoori and T. M. Guo, *SPE J.*, 2004, **41**, 169–182.
11 B. S. Soulgani, B. Tohidi, M. Jamialahmadi and D. Rashtchian, *Energy Fuels*, 2011, **25**, 753–761.
12 P. Zanganeh, S. Ayatollahi, A. Alamdari, A. Zolghadr, H. Dashti and S. Kord, *Energy Fuels*, 2012, **26**, 1412–1419.

13 T. J. Behbahani, C. Ghotbi, V. Taghikhani and A. Shahrabadi, *Fuel*, 2014, **133**, 63–72.
14 N. I. Papadimitriou, G. E. Romanos, G. C. Charalambopoulou, M. E. Kainourgiakis, F. K. Katsaros and A. K. Stubos, *SPE J.*, 2007, **57**, 281–293.
15 X. Q. Wang and Y. A. Gu, *Ind. Eng. Chem. Res.*, 2011, **50**, 2388–2399.
16 M. Cao and Y. A. Gu, *Fuel*, 2013, **109**, 157–166.
17 Z. C. Yu, L. Liu, S. Y. Yang, S. Li and Y. Z. Yang, *Chem. Geol.*, 2012, **326**, 88–101.
18 I. M. Mohamed and H. A. Nasr-El-Din, *Paper SPE 151142, presented at SPE International Symposium and Exhibition on Formation Damage Control*, Lafayette, Louisiana, USA, 15–17 February, 2012.
19 J. Mitchell, L. M. Broche, T. C. Chandrasekera, D. J. Lurie and L. F. Gladden, *J. Phys. Chem. C*, 2013, **117**, 17699–17706.
20 T. C. Wang, N. A. Vermeulen, I. S. Kim, A. B. Martinson, J. F. Stoddart, J. T. Hupp and O. K. Farha, *Nat. Protoc.*, 2016, **11**, 149–162.
21 I. Habina, N. Radzik, T. Topor and A. T. Krzyzak, *Microporous Mesoporous Mater.*, 2017, **252**, 37–49.
22 X. Lu, B. Kalman and P. Redelius, *Fuel*, 2008, **87**, 1543–1551.
23 D. A. Karlsen and S. R. Larter, *Org. Geochem.*, 1991, **17**, 603–617.
24 R. L. Christiansen and K. H. Haines, *SPE Reservoir Eng.*, 1987, **2**, 523–527.
25 P. M. Jarrell, C. Fox, M. Stein and S. Webb, *SPE Monogr.*, 2002, **22**.
26 S. B. Hawthore, D. J. Miller, L. Jin and C. D. Gorecki, *Energy Fuels*, 2016, **30**, 6365–6372.
27 A. M. Elsharkawy, F. H. Poettmann and R. L. Christiansen, *Energy Fuels*, 1996, **10**, 443–449.
28 F. Yang, G. B. Zhao, H. Adidharma, B. Towler and M. Radosz, *Ind. Eng. Chem. Res.*, 2007, **46**, 1396–1401.
29 H. Gao, Y. Liu, Z. Zhang, B. Niu and H. Li, *Energy Fuels*, 2015, **29**, 4721–4729.
30 H. Li, J. Zhu and H. Guo, *Chin. J. Magn. Reson.*, 2008, **25**, 273–280, in Chinese.
31 M. Megawati, M. V. Madland and A. Hiorth, *J. Pet. Sci. Eng.*, 2012, **100**, 123–130.
32 K. R. Brownstein and C. E. Tarr, *Phys. Rev. A*, 1979, **19**, 2446–2453.
33 P. Yang, H. Guo and D. Yang, *Energy Fuels*, 2013, **27**, 5750–5756.
34 M. Megawati, M. V. Madland and A. Hiorth, *J. Pet. Sci. Eng.*, 2012, **100**, 123–130.
35 Z. Q. Mao, Y. D. He and X. J. Ren, *Chin. J. Geophys.*, 2005, **48**, 412–418.
36 F. L. Yang, G. B. Zhao, H. Adidharma, B. Towler and M. Radosz, *Ind. Eng. Chem. Res.*, 2007, **46**, 1396–1401.
37 H. Z. Li, J. S. Qin and D. Y. Yang, *Ind. Eng. Chem. Res.*, 2012, **51**, 3516–3523.
38 R. B. Alston, G. P. Kokolis and C. F. James, *SPE J.*, 1985, **25**, 268–274.